Regular Article

VASCULAR BIOLOGY

Content delivery to newly forming Weibel-Palade bodies is facilitated by multiple connections with the Golgi apparatus

Marjon J. Mourik,[1] Frank G. A. Faas,[1] Hans Zimmermann,[2] Jan Voorberg,[3] Abraham J. Koster,[1] and Jeroen Eikenboom[4]

[1]Department of Molecular Cell Biology, Leiden University Medical Center, Leiden, The Netherlands; [2]Carl Zeiss Microscopy GmbH, Munich, Germany; [3]Department of Plasma Proteins, Sanquin-AMC Landsteiner Laboratory, Amsterdam, The Netherlands; and [4]Department of Thrombosis and Hemostasis, Einthoven Laboratory for Experimental Vascular Medicine, Leiden University Medical Center, Leiden, The Netherlands

---

Key Points

- WPBs stay connected to the Golgi apparatus until vesicle formation is completed.
- During biogenesis at the Golgi, WPBs increase in size through the addition of nontubular VWF.

Weibel-Palade bodies (WPBs) comprise an on-demand storage organelle within vascular endothelial cells. It's major component, the hemostatic protein von Willebrand factor (VWF), is known to assemble into long helical tubules and is hypothesized to drive WPB biogenesis. However, electron micrographs of WPBs at the Golgi apparatus show that these forming WPBs contain very little tubular VWF compared with mature peripheral WPBs, which raises questions on the mechanisms that increase the VWF content and facilitate vesicle growth. Using correlative light and electron microscopy and electron tomography, we investigated WPB biogenesis in time. We reveal that forming WPBs maintain multiple connections to the Golgi apparatus throughout their biogenesis. Also by volume scanning electron microscopy, we confirmed the presence of these connections linking WPBs and the Golgi apparatus. From electron tomograms, we provided evidence that nontubular VWF is added to WPBs, which suggested that tubule formation occurs in the WPB lumen. During this process, the Golgi membrane and clathrin seem to provide a scaffold to align forming VWF tubules. Overall, our data show that multiple connections with the Golgi facilitate content delivery and indicate that the Golgi appears to provide a framework to determine the overall size and dimensions of newly forming WPBs. (*Blood*. 2015;125(22):3509-3516)

Introduction

Rapid secretion of the endothelial storage organelles, the Weibel-Palade bodies (WPBs),[1] is fundamental for hemostasis. WPBs contain the hemostatic glycoprotein von Willebrand factor (VWF), which recruits platelets to sites of injury to arrest bleeding.[2] Within WPBs, VWF is packed into helical tubules that give the organelle an elongated shape with a length of 1 to 5 μm and a width of 100 to 300 nm.[1,3-5] The formation of WPBs is dependent on VWF and also occurs on VWF expression in nonendothelial cells.[6,7] VWF is synthesized in the endoplasmic reticulum as a pre-proprotein consisting of a signal peptide, a propeptide, and mature VWF.[2] On removal of the signal peptide, VWF dimers are formed that are transported to the Golgi apparatus. At the Golgi, the propeptide is cleaved from mature VWF to guide multimerization and tubule formation.[3,8,9] VWF tubule formation is crucial for the development of mature, densely packed elongated WPBs. Mutations in the *VWF* gene, as found in patients with the bleeding disorder von Willebrand disease, were shown to result in altered WPB morphology.[2,10-12] In vitro studies on VWF tubule formation demonstrated that the core of the VWF tubules is formed by the propeptide and the N-terminal D′ and D3 assembly of mature VWF.[3] However, it is still poorly understood how the formation of the VWF tubules is related to WPB biogenesis.

Electron microscopy studies have revealed several stages in the WPB formation process. At the Golgi, immature WPBs were observed ranging from small WPB-like vesicles of about 200 to 400 nm long containing 2 to 3 tubules, to larger immature WPB several microns long that contained numerous tubules.[13] Immature WPBs are typically extensively decorated by clathrin. Clathrin possibly acts as an external scaffold for the forming vesicle and appeared to be essential for WPB biogenesis.[14,15] As WPBs are formed, the VWF content increases and becomes condensed. However, it is still unclear how this is achieved. Electron tomography on irregular-shaped WPBs indicated that postbudded WPBs may increase size by homotypic fusion.[16] Recently, it was postulated that WPB size is fully determined by the Golgi apparatus by packaging so-called VWF "quanta" into newly forming WPBs.[17]

In the present study, we applied several electron microscopic techniques to study early steps in WPB biogenesis in vascular endothelial cells. We show that newly forming WPBs contain multiple connections to the Golgi apparatus that seem to facilitate WPB growth by transporting nontubular VWF clusters from the Golgi to the WPB lumen.

Methods

Cell culture and transfection

Human umbilical vein endothelial cells (HUVECs; Lonza, Walkersville, MD) were cultured in endothelial growth medium-2 (EGM-2 bulletkit; Lonza) to 100% confluence in 1% gelatin-coated culture flasks. Transfection was performed using the HUVEC Nucleofector Kit (Lonza). For each reaction we used 2 μg DNA, 1×10^6 cells, and program A-034. To increase cell survival after transfection, the growth medium was supplemented with 20% fetal calf serum. Cells were transfected with propeptide-enhanced green fluorescent protein (EGFP; from Prof Carter, St. George University of London, London, UK).[18]

WPB formation after exocytosis

Cells cultured on glass coverslips and sapphire disks were stimulated with 80 nM phorbol 12-myristate 13-acetate (PMA) as previously described.[19] Control cells were incubated simultaneously in medium containing the vehicle only. Cells were subsequently washed with incubation medium and EGM-2. The cells were then allowed to recover for 0, 2, 4, 6, and 8 hours. At each time point, sapphire disks were cryo-immobilized by high pressure freezing and coverslips were fixed in 3% paraformaldehyde in 0.1 M phosphate buffer, pH 7.4, for 30 minutes.

Confocal microscopy

Fixed cells were washed in 50 mM Tris HCl, pH 7.4, and permeabilized with 0.1% Triton X-100 in phosphate-buffered saline (PBS). After blocking with PBS 5% normal goat serum, the cells were incubated with primary and secondary antibodies. Nuclei were stained with DraQ5 (Biostatus) or 4′,6-diamidino-2-phenylindole, dihydrochloride (Invitrogen Molecular Probes, Eugene, OR). Coverslips were mounted on glass slides with Aquapolymount (Omnilab, Warrington, PA). Primary antibodies were fluorescein isothiocyanate (FITC)-conjugated sheep anti-VWF antibody (Abcam, Cambridge, UK), rabbit polyclonal anti-TGN46 (Abcam), mouse monoclonal anti-LAMP1 (mAb BB6; kindly provided by Dr S. Carlsson, Umeå, Sweden), and mouse monoclonal anti-EEA-1 (BD Biosciences, San Jose, CA). Secondary antibodies were Alexa 568-conjugated goat anti-mouse (Invitrogen Molecular Probes). Samples were imaged on a Leica SP5 or a Leica SP8 (Leica Microsystems, Wetzlar, Germany) using a ×63/NA 1.4 oil immersion objective.

Immunogold detection of VWF containing structures

Cryo-immobilized samples were processed by freeze substitution according to Kukulski et al[20] using acetone with 0.1% uranly acetate. Samples were infiltrated and embedded in Lowicryl HM20. Sections of 100 to 120 nm were placed on Formvar and carbon-coated electron microscopy grids. For labeling, the sections were incubated with polyclonal anti-VWF antibodies (Dako, Glostrup, Denmark) diluted in PBS, 0.8% bovine serum albumin, and 5% fetal calf serum and subsequently in PBS, 0.8% bovine serum albumin, and 5% fetal calf serum containing protein A-gold 15-nm particles. Sections were contrasted with 7% uranyl acetate. Immunogold labeling was imaged using a Tecnai 12 transmission electron microscope (TEM) at 120 kV (FEI Company, Eindhoven, The Netherlands) equipped with a 4k × 4k CCD camera (Model Eagle; FEI Company). Large mosaics scans were collected using MyMesh/MyStitch software,[21] which were analyzed and annotated using ImageScope (Aperio Technologies, Vista, CA).

Correlative light and electron microscopy

To localize cells, finder grid patterns were carbon coated in CellView AdvancedTC glass bottom dishes (Greiner, Bio One GmbH, Frickenhausen, Germany) as described.[22] The dishes were sterilized with UV and coated with 1% gelatin. Transfected cells were seeded and were allowed to express the construct for 2, 4, 6, 8, and 10 hours. Cells were fixed with 2% paraformaldehyde and 0.5% glutaraldehyde in 0.1 M phosphate buffer, pH 7.4. For relocation purposes, the nuclei were stained with DraQ5 (Biostatus, Shepshed, UK). Cells were imaged with a Leica SP5 confocal laser scanning microscope equipped with a ×63/NA 1.4 oil immersion objective. Deconvolution was performed using Huygens Pro software (Scientific Volume Imaging, Hilversum, The Netherlands). TEM samples were processed as described.[23] Correlated fluorescence and electron micrographs were overlaid in Adobe Photoshop CS6 (Adobe Inc, San Jose, CA) using the nuclei in the area of interest to align the two images. For electron tomography, 10-nm gold fiducials were added to the samples. Dual-axis tilt series were collected with SerialEM[24] using tilt angles from −60° to +60°, with a 1° increment. Tomograms were reconstructed and combined using IMOD.[25] Segmentations were created with Amira (Visualization Sciences Group, FEI Company).

Volume scanning electron microscopy

Cells were grown on Thermanox coverslips (Thermo Scientific, Hudson, NH). On confluence, the cells were fixed with 1.5% glutaraldehyde in 0.1 M cacodylate buffer, pH 7.4, for at least 1 hour. Further processing was performed as previously described.[26] Resin-filled capsules were placed on top of the cells and were polymerized for 48 to 72 hours at 60°C.

The cells were imaged using an Auriga CrossBeam (Carl Zeiss Microscopy GmbH, Munich, Germany) scanning electron microscope (SEM) at an acceleration voltage of 1.7 kV and a beam current of 220 pA. Images were acquired using both the InLens secondary electron detector and the energy-selected backscattered electron detector. For focused ion beam milling, a milling current of 4 nA and an acceleration voltage of 30 kV were used.

The raw data stack was aligned by phase correlation with a Gaussian window function. Although the data show indications of local deformations, correcting for image shifts was sufficient for our purposes. Segmentation was performed using Amira (Visualization Sciences Group, FEI Company).

Results

Immunolabeling on TEM sections reveals early stages in WPB biogenesis

To explore the morphological changes of newly forming WPBs at the Golgi, we first depleted WPBs by inducing their release from endothelial cells. Cells were stimulated for 20 minutes with 80 nM PMA, washed, and left to recover for 0 to 8 hours. After 0, 2, 4, 6, and 8 hours of recovery, control and PMA-treated cells were fixed and analyzed by confocal microscopy. Parallel samples were cryo-immobilized by high pressure freezing for freeze substitution.

Confocal analysis revealed normal exocytosis patterns of VWF strings and rounded WPBs after 0 hours of recovery. Control cells showed a normal WPB distribution (supplemental Figure 1, available on the *Blood* Web site). We found that after 2 hours of recovery, the PMA-treated cells were devoid of any WPBs, and no WPB-like vesicles were detected at the Golgi apparatus (Figure 1A). In the periphery of the cells, some residual VWF staining was observed, which mainly colocalized to lysosomes as shown by colabeling with the lysosomal LAMP-1 marker (supplemental Figure 1). After 4 hours of recovery, the first WPB-like structures were observed at the Golgi region (Figure 1A). Staining was often quite faint, and vesicles were relatively small compared with mature WPBs. The amount of vesicles in proximity of the Golgi region increased after 6 hours of recovery, and more elongated structures were observed (Figure 1A). Only a few WPBs were present in the periphery of the cell. After 8 hours of recovery, larger numbers of peripheral WPBs

Figure 1. Formation of WPBs in HUVECs after PMA stimulation. HUVECs stimulated with PMA were washed with medium and were left to recover for 2 to 8 hours. (A) Immuno-fluorescent labeling for VWF (VWF-FITC, green channel), the *trans*-Golgi network (TGN 46 Alexa 568, red channel), and the nucleus (4′,6-diamidino-2-phenylindole, dihydrochloride, blue channel) after 2, 4, 6, and 8 hours of recovery. We found that the cells were devoid of WPBs after 2 hours of recovery. We followed the production of new WPBs from that time point onward. (B-G) VWF-specific immunogold labeling on TEM samples prepared after 2, 4, 6, and 8 hours of recovery. Gold particles are 15 nm in size. (B-C) Immuno-gold labeled structures found after 2 hours of recovery. (B) Large vesicle found close to the cell membrane that contains VWF specific immunogold label. (C) Lysosome-like structure showing VWF specific immunolabeling. (D-Di) Immature WPBs positively labeled for VWF near the Golgi apparatus (Go) that was found in TEM samples prepared after 4 hours of recovery. (E-Ei) A more advanced immature WPB positively labeled for VWF that was found close to the Golgi (Go) in TEM samples prepared after 6 hours of recovery. In this WPB, longer VWF tubules are observed compared with the 4-hour condition. (F) Condensed mature WPBs found after 8 hours of recovery. (G) VWF-containing vesicle found after 8 hours of recovery that appears to contain disorganized VWF tubules. Scale bars: (A) 5 μm; (B-G) 250 nm. Fluorescence images were acquired using a Leica SP5 or Leica SP8 confocal with a ×63 oil immersion objective with a numerical aperture of 1.4. Fluorochromes used are FITC (conjugated to sheep anti-VWF antibodies, green), Alexa 568 (conjugated to goat anti-rabbit antibodies, red), and DraQ5 (blue). Electron micrographs were acquired using an FEI Tecnai 12 at 120 kV and using an FEI Eagle 4k × 4k CCD camera.
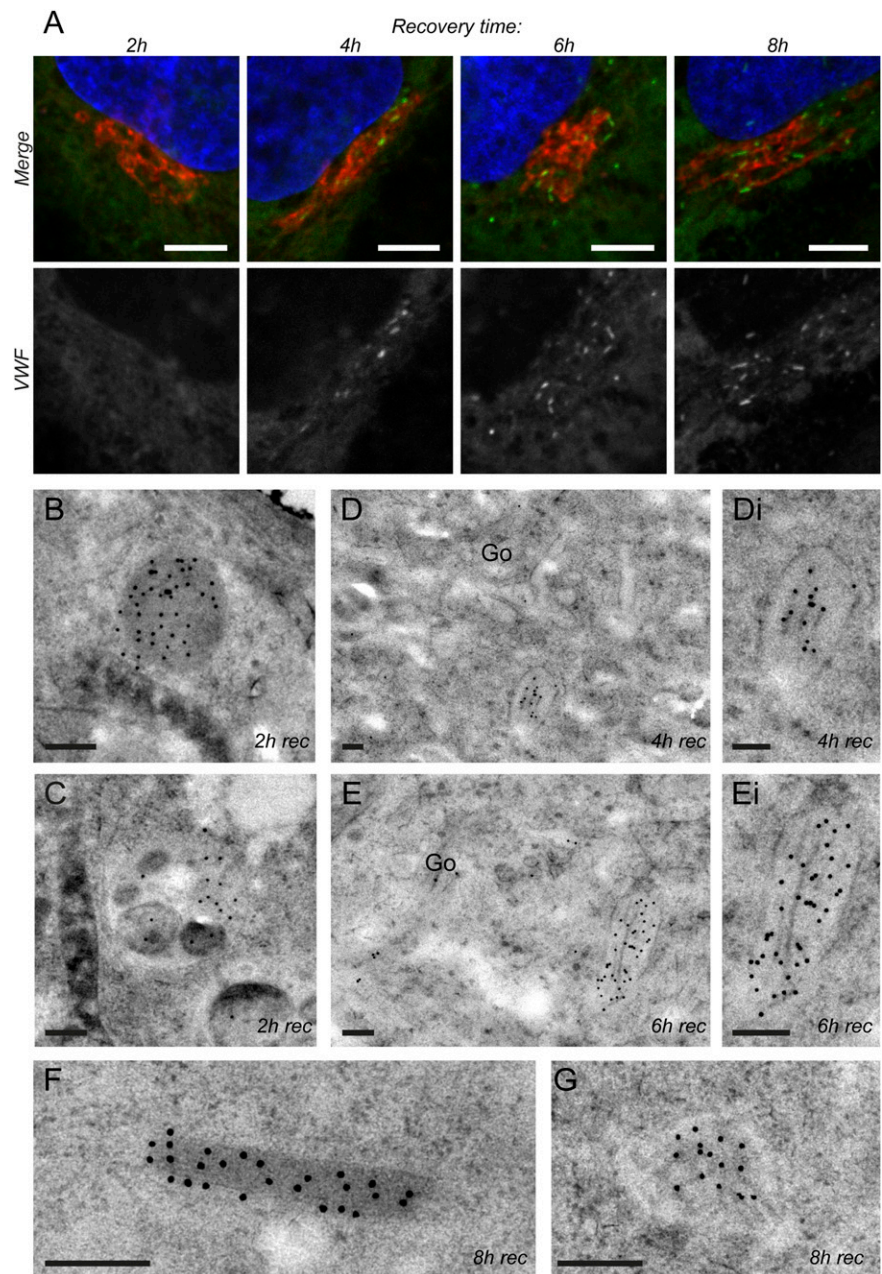
were detected, indicating that the early stages of WPB formation were completed. For TEM analysis, we therefore mainly focused on the time points of 2 to 8 hours.

Similarly treated samples were processed for TEM by freeze substitution to enable VWF specific immunogold labeling on resin section. Consistent with the fluorescence data, we observed the VWF-specific labeling after 2 hours of recovery, mainly in lysosome-like vesicles or in large, possibly endosomal, vesicles (Figure 1B-C). The internal morphology and the widely spread localization of the vesicles suggested that these vesicles were not involved in WPB biogenesis. The first WPB-like structures were found after 4 hours of recovery. At the Golgi area, a 500-nm-long vesicle was found containing several tubules, which were decorated with gold particles (Figure 1D-Di). After 6 hours of recovery, larger immature WPBs were found (Figure 1E-Ei). In cells that were left to recover for 8 hours, mainly matured WPBs were found that had moved away from the Golgi (Figure 1F). Next to the vesicles that clearly resembled WPBs, other vesicles were found

that seemed to contain disorganized VWF material. These vesicles were mainly found after 6 to 8 hours of recovery and may represent incorrectly folded WPBs or vesicles following constitutive secretion route (Figure 1G).

Morphological analysis of forming WPBs by correlative light and electron microscopy

The above-described sample preparation method for immunogold labeling on TEM specimens allowed the detection of VWF containing newly forming WPBs but revealed limited morphological information. To obtain more information on the positioning of immature WPBs with respect to the Golgi apparatus, we additionally performed correlative light and electron microscopy (CLEM), in which confocal scanning laser microscopy was combined with conventional TEM sample preparation and electron tomography. To label WPBs, we transfected HUVECs with the propeptide of VWF (D1-D2 domains)
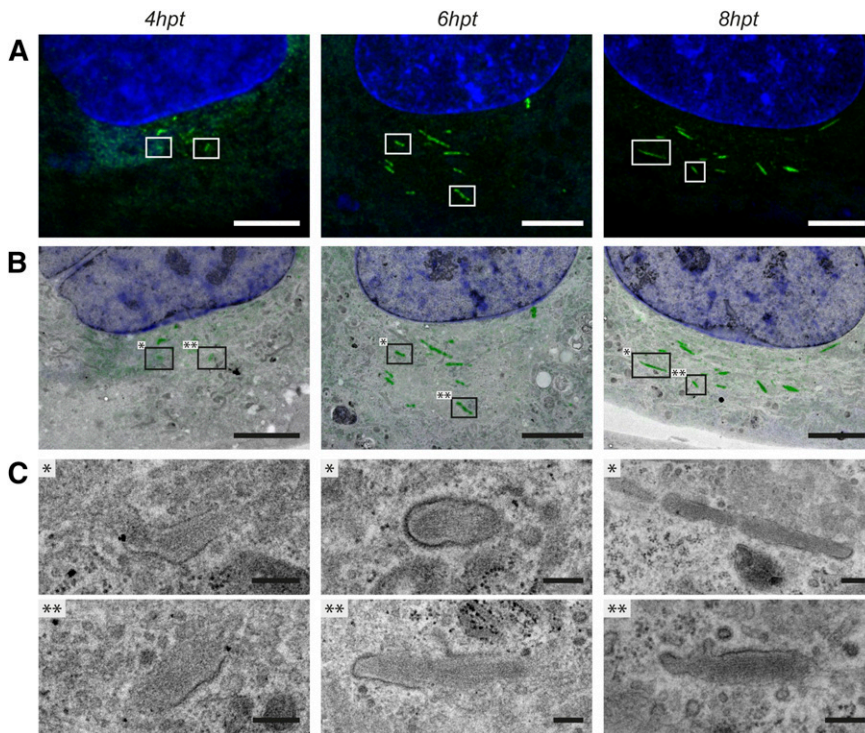
Figure 2. Correlative light and electron microscopy on forming WPBs in propeptide-EGFP transfected HUVECs. HUVECs transfected with propeptide-EGFP were fixed at several time points after transfection for CLEM. (A) Fluorescence images of HUVECs showing forming WPBs 4, 6, and 8 hours after transfection (hpt) (green channel). The nuclei were stained with DraQ5 (blue channel). The presented images are maximum intensity projections of deconvoluted z-stacks. The boxed WPBs represent 2 examples that were correlated to the corresponding TEM sample as shown in B and C. (B) Overlay of the fluorescence image shown in A and the electron micrograph of a corresponding TEM section. Boxes with asterisks represent 2 examples of WPBs in which the morphology is shown in C. (C) Electron micrographs of correlated WPBs. After 4 hours of transfection, the immature WPBs display a very electron lucent lumen. After 6 and 8 hours of transfection, the WPB lumen becomes more condensed. Also the VWF tubules become more visible within the lumen of the WPB. Scale bars: (A-B) 5 μm; (C) 250 nm. Fluorescence images were acquired using a Leica SP5 confocal with a ×63 oil immersion objective with a numerical aperture of 1.4. Fluorochromes used are EGFP tagged to the propeptide of VWF (propeptide-EGFP, green) and DraQ5 (blue). Deconvolution of the confocal images was performed using Huygens Pro. Electron micrographs were acquired using an FEI Tecnai 12 at 120 kV and using an FEI Eagle 4k × 4k CCD camera. Overlays as shown in B were prepared in Adobe Photoshop CS6.

fused to EGFP (propeptide-EGFP).[18] The EGFP-tagged propeptide becomes incorporated in forming WPBs. To follow the consecutive steps in WPB biogenesis, cells were fixed after 2, 4, 6, 8, and 10 hours after transfection for CLEM analysis. Newly formed WPB-like structures were first visible after 4 hours of transfection (Figure 2A). Typically, a cluster of small slightly elongated structures was observed. The fluorescence signal of these immature WPBs was low compared with the WPBs found in later stages. After 6 and 8 hours of transfection, more developed WPBs were observed that were larger and more elongated (Figure 2A). Interestingly, these large WPBs still seemed to localize to the Golgi region (Figure 2A). The first propeptide-EGFP labeled WPBs close to the edge of the cell were observed in cells that were fixed after 10 hours of transfection (supplemental Figure 2).

Following confocal imaging, samples were processed for TEM analysis. As our questions relate to the processes occurring at the Golgi, we concentrated on the early time points from 4 to 8 hours after transfection. To correlate the imaged fluorescence to corresponding structures in the TEM samples, we first relocated the previously imaged cells in consecutive TEM sections and overlaid the fluorescence image with electron micrographs (Figure 2B). Electron lucent clathrin-decorated immature WPBs were found 4 hours after transfection (n = 6; Figure 2C; supplemental Figure 2). These immature WPBs did not seem to contain very clear VWF tubules. Similar immature WPBs were also found after 6 hours of transfection (n = 4). However, the majority of the correlated WPBs were elongated (n = 8; Figure 2C; supplemental Figure 2). The WPBs that were formed in 8 hours (n = 14) of transfection appeared even more elongated and appeared denser than WPBs found after 6 hours of transfection.

Immature WPBs are linked to the Golgi apparatus through multiple connections

WPBs identified by CLEM were often found in close proximity to Golgi stacks. However, in the 2-dimensional images, connections with

the Golgi were difficult to distinguish (Figure 3A). Previous studies using advanced TEM preparation techniques already showed that there are connections between the proximal end of WPBs and the Golgi.[13] To further study the spatial organization of forming WPBs at the Golgi apparatus, we used dual-axis electron tomography. From each condition, we selected 3 to 4 WPBs of various sizes for 3-dimensional analysis. Strikingly, the electron tomograms revealed that the immature WPBs formed in 4 hours of transfection are tightly associated with the Golgi via numerous connections (see arrows in Figure 3B-C; supplemental Video 1). These connections were found at the tips of the elongating WPBs but also on the lateral side of the granule. To show all the connections to the Golgi, we created a 3-dimensional model of the WPB membrane (Figure 3D; supplemental Video 1). In addition we also created a 3-dimensional model that included both Golgi membranes and the immature WPB (Figure 3E). This image confirmed that multiple connections were present between the Golgi apparatus and immature WPBs. In these early WPBs, the internal organization of VWF is disorganized and only partially tubulated (supplemental Video 1). The clathrin coat, which is thought to support the membrane during formation, was mainly observed on parts of the granule that were devoid of connections to the Golgi (Figure 3B-C).

When analyzing tomograms collected from correlated WPBs in cells fixed after 6 and 8 hours of transfection, we noticed to our surprise that the WPBs still were connected to the Golgi. Figure 4A shows a 2-dimensional electron micrograph of 3 supposedly individual WPBs that were formed in 8 hours of transfection. Tomography on these structures revealed that these 3 parts are actually a single WPB of almost 2.5 μm in length (Figure 4B; supplemental Video 2) displaying several connections to the neighboring Golgi stack (see arrows in Figures 4C-E). At this stage, the WPB is still extensively decorated by clathrin but has acquired a remarkably tubular and condensed internal organization, which indicates that even these relatively mature WPBs maintain linked to the Golgi apparatus.

Figure 3. Electron tomography reveals numerous connections between the Golgi apparatus and WPBs found after 4 hours of transfection. Example of a WPB 4 hours after transfection displaying numerous connections to the Golgi when analyzed by electron tomography. The WPB was localized using CLEM. (A) Two-dimensional image of an immature WPB that was observed in close proximity to the Golgi. (B-C) Tomogram sections showing the connections (arrows) to the Golgi. Also note that the membrane that is not associating with the Golgi is coated by clathrin (arrowheads). (D) A 3-dimensional model of the forming WPB (green) showing the numerous connections (arrows). (E) The addition of a 3-dimensional representation of the Golgi (light yellow) reveals its complex organization around the forming WPB (green). See also supplemental Video 1. Scale bars: (A-B) 250 nm. Electron micrographs and tilt series for tomography were acquired using an FEI Tecnai 12 at 120 kV and using an FEI Eagle 4k × 4k CCD camera. Tilt series for tomography were collected with SerialEM. Tomogram reconstructions were performed in IMOD. Segmentation was performed in Amira (Visualization Sciences Group, FEI). Go, Golgi.
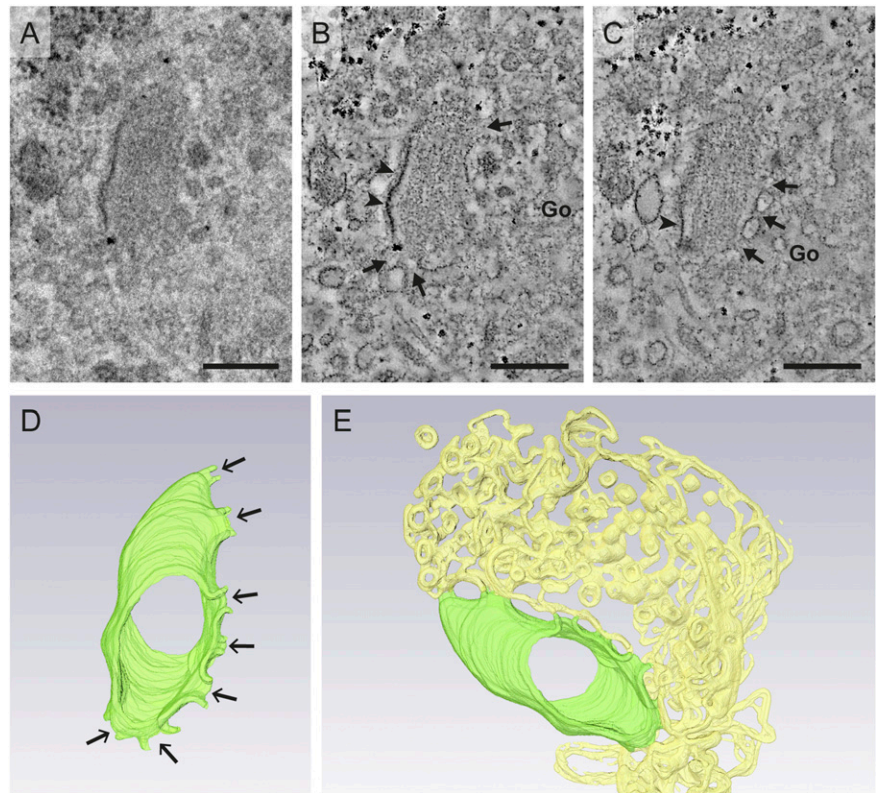
Adding nontubular VWF to the forming WPBs enables vesicle growth

The acquired tomograms to study the relationship between the Golgi apparatus and the forming WPBs also provided new information on vesicle growth during WPB formation. Tomograms of correlated WPBs formed in 4 hours of transfection revealed clusters of nontubular VWF that were added to the proximal end of the WPBs in the transition from Golgi to WPB lumen (Figure 5A-Ai; indicated by nt). The transition from VWF multimers to VWF tubules would in that case occur within forming WPBs and could explain why the tubules are initially disorganized in immature WPBs.

Addition of VWF clusters to forming WPBs via more lateral connections was observed after 8 hours of transfection (Figure 5B-Bii). At this stage, signs of fusion were observed, as irregular-shaped WPBs were visualized by electron tomography (Figure 4A-B). Interestingly, the irregular-shaped WPBs were still connected to the Golgi, suggesting that fusion occurs while the connections are maintained. We also observed small vesicles containing a single tubule next to already formed WPBs (Figure 5C). These vesicles may be added to forming WPBs as some of the correlated WPBs showed irregularities that suggested fusion with such a small vesicle (Figure 5D).

Clathrin-mediated membrane retrieval shapes the WPBs into tightly packed cigar

Clathrin is known to play an important role in WPB formation.[13-15] It is proposed to act as a scaffold to support the vesicle but was also reported to play a role in excess membrane retrieval to condense the VWF tubules in WPBs.[13,14] The WPBs that we studied by CLEM also displayed pronounced clathrin coats. On WPBs formed in 4 hours of transfection, the clathrin coat was mainly observed as a lattice along the vesicle membrane (Figure 5A-Ai). However, at the areas where connections between the forming WPB and Golgi were found,

discontinuities in the clathrin coat were observed. This pattern of clathrin coating was seen on WPBs at up to 8 hours of development and even on large WPBs. After 6 hours of transfection, the first clathrin-coated pits were observed in WPB membranes (Figure 5E), which may represent the initiation of WPB condensation. Budding of clathrin-coated vesicles from irregularly shaped WPBs may force further compaction of VWF tubules into highly organized tubular assemblies as observed in peripheral WPBs. More pronounced profiles of budding clathrin-coated vesicles (Figure 5F) were observed after 8 hours of transfection.

Three-dimensional analysis of the Golgi and the relationship with forming WPBs

Finding immature WPBs in TEM samples of native HUVECs without the use of CLEM can be challenging and time consuming. Volume-SEM was used to study the 3-dimensional organization of forming WPBs at the Golgi apparatus. For this technique, cells are extensively stained with metal and embedded in resin. In the SEM, cells are imaged perpendicular to the growing surface while a focused ion beam removes thin 10-nm slices. Imaging and removing material from the block is repeated automatically until the preferred volume is imaged. A difference compared with TEM micrographs is that the contrast of the SEM images is inverted. To visualize WPBs at the Golgi apparatus, we imaged a volume of $11.4 \times 8.5 \times 16$ μm. The images were aligned, analyzed, and modeled as shown in Figure 6 and supplemental Video 3. Figure 6A shows the model of an imaged endothelial cell. The nucleus is depicted in dark blue, the cell membrane is shown in cyan, and the Golgi apparatus is shown in green. WPBs modeled in red were found to be closely associated with the Golgi apparatus. Peripheral WPBs are shown in orange. Figure 6B shows one of the imaged slices and reveals a mature WPB at the cell membrane and an immature WPB at the Golgi. The immature WPB shows a connection with the Golgi (Figure 6C-Ci).
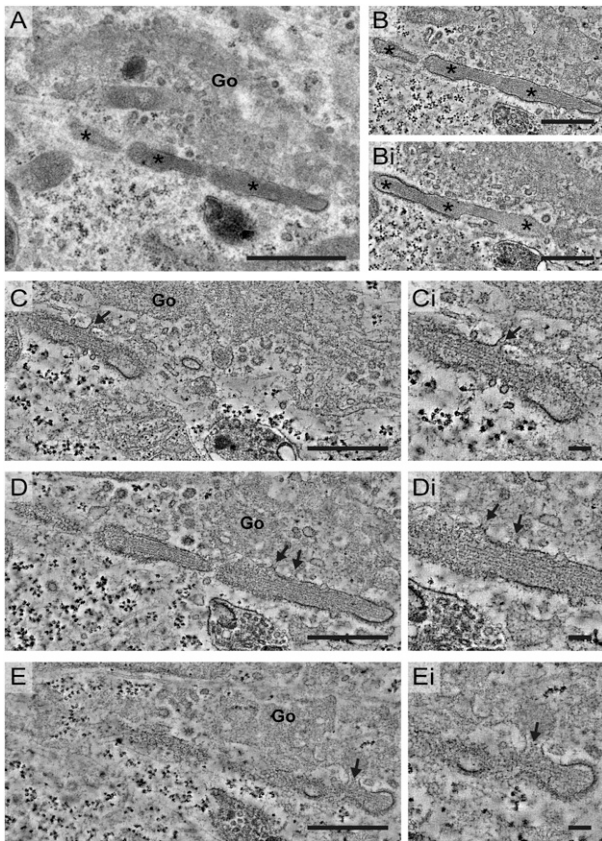
Figure 4. WPBs stay connected to the Golgi until vesicle formation is completed. WPBs 8 hours after transfection localized by CLEM and analyzed by electron tomography. (A) Two-dimensional image of 3 supposedly individual WPBs (asterisk) in close proximity to the Golgi. (B-Bi) Tomogram sections that reveal the continuous membrane around an irregular-shaped WPB, which is formed by 3 parts (asterisk) indicated in A. (C-E) Tomogram sections showing the connections (arrows) between the Golgi and the WPB. (Ci-Ei) Zoom of the connections (arrows) shown in C-E. See also supplemental Video 2. Scale bars: (A) 1 μm; (B-Bi and C-E) 500 nm; (Ci-Ei) 100 nm. Electron micrographs and tilt series for tomography were acquired using an FEI Tecnai 12 at 120 kV and using an FEI Eagle 4k × 4k CCD camera. Tilt series for tomography were collected with SerialEM. Tomogram reconstructions were performed in IMOD. Go, Golgi.

In addition a few VWF tubules are observed in the lumen of the immature WPB (Figure 6Cii). When the volume is analyzed in different orientations, WPBs are observed that appear to have multiple connections with the Golgi (Figure 6D-Dii).

Discussion

In the present study, we provide evidence for a novel WPB biogenesis model in which newly formed WPBs maintain multiple connections with the Golgi apparatus until vesicle formation is completed. We characterized forming WPBs by the analysis of immunogold-labeled TEM sections, CLEM, and volume-SEM. The CLEM results showed that the earliest examined WPBs displayed multiple connections to the Golgi at both ends. These connections appeared to be maintained during development because large 2.5-μm-long compact VWF tubule-containing WPBs were still found to be connected to the Golgi (Figure 4D).

Similar to Ferraro et al,[17] our results support the hypothesis that the Golgi tightly regulates WPB size by combining several smaller WPBs. We visualized that clusters of nontubulated material appear to be added to forming WPBs (Figure 5A-B), which provided evidence for a novel

mechanism for WPB formation and WPB growth. Adding nontubular VWF to forming WPBs enables the Golgi to transport relatively large quantities of VWF required for WPB formation. We therefore hypothesize that WPB formation initially starts with the aggregation of VWF multimers in specialized Golgi areas that evolve into WPBs in which a suitable pH and calcium concentration is created to initiate tubule formation.[3] Evidence for this hypothesis is found in our tomograms on early staged immature WPBs, which revealed areas with VWF that were partially tubulated and partially in an intermediate or nontubulated conformation (Figure 5A-Ai). This observation suggested that tubule formation occurs in the lumen of the WPB and that not all tubules are made at once; nontubulated VWF clusters can be converted into tubules independently of the presence of preformed tubules in immature WPBs. This could explain why immature WPBs often display disorganized
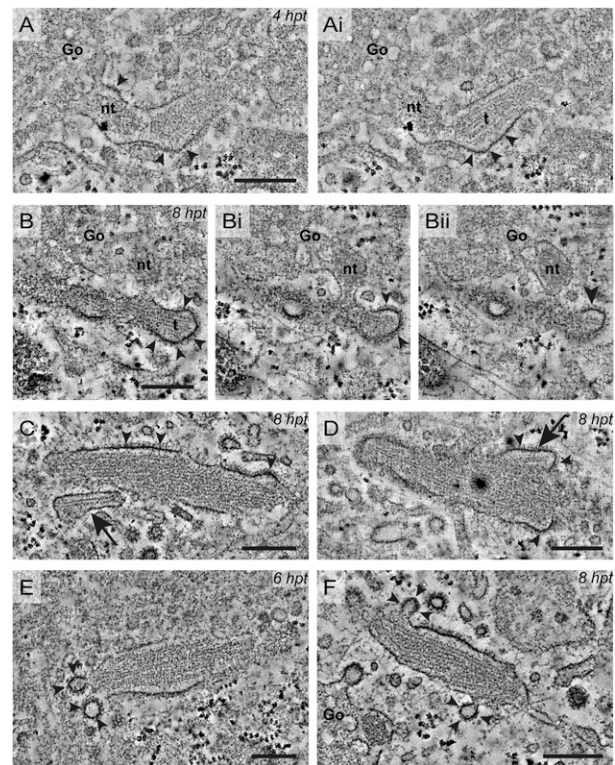

Figure 5. WPB growth is achieved by adding nontubulated VWF to the vesicle lumen. WPB elongation and condensation occurs by clathrin-mediated membrane remodeling. Electron tomograms of WPBs localized by CLEM revealed insights in mechanisms that seem to contribute to WPB growth, elongation, and membrane remodeling. (A-Ai) Tomogram sections of a WPB formed 4 hours after transfection (hpt). In the transition from Golgi to the forming WPB, a dense cluster of nontubulated VWF is observed, whereas VWF in the WPB lumen is tubulated (t). Also note the clathrin coat on the membrane of the WPB (arrowheads). (B-Bii) Tomogram sections of a WPB 8 hpt. In the Golgi, a dense cluster of nontubulated VWF is visible, which seems to be delivered to the forming WPB via the connection visible between the Golgi and WPB membrane. In the WPB tubules of VWF (t) are observed. The arrowheads indicate the extensive clathrin coat observed on the WPB membrane. This WPB is also presented in Figiugre 4E-Ei. (C) Tomogram section of a WPB 8 hpt. Close to the WPB, a small vesicle is observed that contains one tubule (arrow). On the WPB membrane, an extensive clathrin coat is observed (arrowheads). (D) Tomogram section of a WPB 8 hpt. The irregular shaped membrane (arrow) suggests fusion between the WPB and vesicles as shown in C. Also, an abundant clathrin coating (arrowheads) was observed on the WPB membrane. (E) Tomogram section of a WPB 6 hpt. In the WPB membrane, clathrin-coated pits are observed (arrowheads), which suggest clathrin-mediated compensatory membrane retrieval. (F) Tomogram section of a WPB 8 hpt close to the Golgi apparatus. On the WPB membrane, more pronounced clathrin-coated pits are observed as indicated by the arrowheads. Scale bars: 250 nm. Tilt series for tomography were acquired using an FEI Tecnai 12 at 120 kV and using an FEI Eagle 4k × 4k CCD camera. Tilt series for tomography were collected with SerialEM. Tomogram reconstructions were performed in IMOD. Go, Golgi; nt, nontabulated.
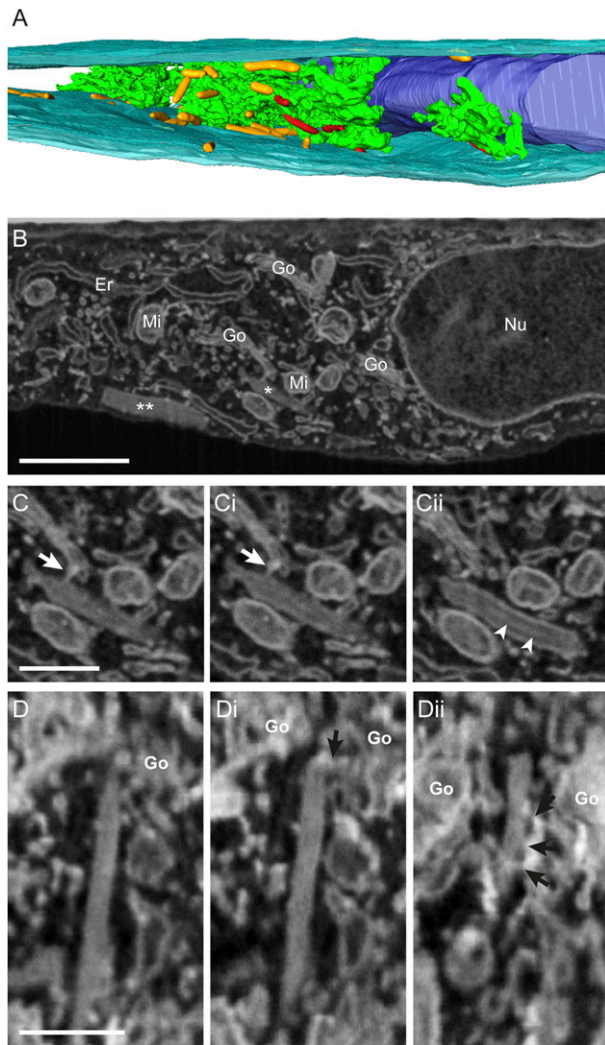
Figure 6. Volume scanning electron microscopy reveals tight associations between forming WPBs and the Golgi apparatus in native HUVECs. The Golgi area was examined and imaged using focused ion beam scanning electron microscopy (FIB-SEM). (A) Three-dimensional model of the total imaged volume: 11.4 × 8.5 × 16 μm. The Golgi apparatus is shown in green; the WPBs associating with the Golgi are in red; peripheral WPBs are in orange; nucleus is in dark blue; and the cell membrane is shown in light blue. (B) FIB-SEM slice showing the Golgi, an associating immature WPB (*), and mature WPBs (**). Note that the mature WPB is much brighter due to its concentrated protein compared with the immature WPBs. The nucleus (Nu), the endoplasmic reticulum (Er), and the mitochondria (Mi) are also visible. (C-Cii) Series of slices from the imaged volume to show the tight association between the Golgi and an immature WPB. The data are shown in the x-y orientation. (C-Ci) Connection between the immature WPB and the Golgi (arrow). (Cii) A few VWF tubules (arrowheads) in the lumen of the immature WPB. (D-Dii) Series of slices from the imaged volume to show multiple associations between the Golgi and a single immature WPB. The data are shown in the x-z orientation. (D) Immature WPB in close proximity with the Golgi. (Di) Connection between the top part of the WPB and the Golgi. (Dii) Additional connections with the Golgi along the membrane of the WPBs, which were found at the bottom of the WPBs. See also supplemental Video 3. Scale bars: (A) 1 μm; (C-D) 500 nm. Volume-SEM data were acquired using an Auriga CrossBeam (Carl Zeiss Microscopy GmbH) SEM at an acceleration voltage of 1.7 kV and a beam current of 220 pA. Images were acquired using both the InLens secondary electron detector and the energy selected backscattered electron detector. Data were collected at ×25 000 magnification. Segmentation was performed in Amira (Visualization Sciences Group, FEI). Go, Golgi.

tubules. We postulate that the Golgi membrane itself, possibly together with clathrin, initiates the formation of an elongated WPB by creating a mold to guide parallel VWF tubule formation. Previously, Lui-Robers et al[14] showed the necessity of AP-1 and clathrin in WPB formation by demonstrating that knockdown of AP-1 or clathrin resulted in perturbed

WPB biogenesis.[14] Once sufficiently long VWF tubules are formed, the VWF tubules maintain the elongated shape. At this point, the clathrin coat can be removed, and the WPBs are ready to leave the Golgi for further maturation.

Another mechanism that could result in vesicle growth is homotypic fusion between small WPBs as proposed previously.[16] Our data suggest that large WPBs as shown in Figure 4 are the result of fusion between WPBs that were connected to the Golgi. Ferraro et al[17] recently showed by live cell imaging that homotypic fusion indeed occurs between WPBs at the Golgi. We did not find examples of post-Golgi homotypic fusion between WPBs.

Our findings underline the crucial role of the Golgi as the supplier of WPB content at different stages of their biogenesis. During this process, a protein flux toward the storage organelle is expected. Our results indicate that nontubular VWF is mainly added via the proximal connections with the WPB, suggesting that the other cargo is added via the smaller lateral connections. In view of the multiple connections between Golgi stacks and WPBs, it is likely that a considerable number of secretory proteins present in the Golgi can enter newly forming WPBs by a default pathway. Removal of cargo that cannot be accommodated in the tubular architecture of WPBs is most likely removed by vesicles involved in clathrin-mediated compensatory membrane retrieval (Figure 5D-F). The dynamics between the Golgi and the forming WPBs are intriguing. We and others have observed, by live cell imaging, that WPBs at the Golgi apparatus are very motile and tend to move along the Golgi.[17] Therefore, the connections between Golgi and WPBs are possibly highly flexible and may exist only for short times, for instance, to add more VWF or other cargo.

Our study provides the first data on the spatial organization of newly forming WPBs near the Golgi apparatus, which may explain why previous electron microscopy studies into WPB formation resulted in a different biogenesis model. The study from Zenner et al[13] on WPBs at the Golgi did reveal stalk-like connections at the proximal ends of WPBs, suggesting that WPBs emerge from VWF tubules that push the Golgi membrane outward. However, they could not reveal how immature WPBs increase in VWF content. The electron tomography study from Valentijn et al[16] on mature WPBs provided evidence of homotypic fusion, resulting in the hypothesis that immature WPBs fuse with each other to concentrate VWF in larger organelles. However, the observations of Valentijn et al[16] could also be the result of Golgi-mediated fusion between forming WPBs.

In conclusion, the data presented in our study support a novel model for WPB biogenesis. This model provides a mechanism for vesicle growth and explains the observed morphological changes that occur during WPB formation. In short, our data indicate that granule formation is initiated in a distinct Golgi stack where clusters of VWF multimers aggregate and tubulate. During this process, the Golgi membrane forms a scaffold structure with clathrin to create an elongated organelle in which the VWF tubules are formed and aligned into a parallel organization. The emerged WPB remains attached to the Golgi through multiple connections to allow further addition of VWF and other cargo proteins until WPB formation is completed.

Authorship

Correspondence: Jeroen Eikenboom, Leiden University Medical Center, P.O. Box 9600, 2300 RC Leiden, The Netherlands; e-mail: h.c.j.eikenboom@lumc.nl.

References

1. Weibel ER, Palade GE. New Cytoplasmic Components in Arterial Endothelia. *J Cell Biol.* 1964;23(1):101-112.

2. Valentijn KM, Eikenboom J. Weibel-Palade bodies: a window to von Willebrand disease. *J Thromb Haemost.* 2013;11(4):581-592.

3. Huang RH, Wang Y, Roth R, et al. Assembly of Weibel-Palade body-like tubules from N-terminal domains of von Willebrand factor. *Proc Natl Acad Sci USA.* 2008;105(2):482-487.

4. Valentijn KM, Sadler JE, Valentijn JA, Voorberg J, Eikenboom J. Functional architecture of Weibel-Palade bodies. *Blood.* 2011;117(19):5033-5043.

5. Berriman JA, Li S, Hewlett LJ, et al. Structural organization of Weibel-Palade bodies revealed by cryo-EM of vitrified endothelial cells. *Proc Natl Acad Sci USA.* 2009;106(41):17407-17412.

6. Michaux G, Hewlett LJ, Messenger SL, et al. Analysis of intracellular storage and regulated secretion of 3 von Willebrand disease-causing variants of von Willebrand factor. *Blood.* 2003; 102(7):2452-2458.

7. Voorberg J, Fontijn R, Calafat J, Janssen H, van Mourik JA, Pannekoek H. Biogenesis of von Willebrand factor-containing organelles in heterologous transfected CV-1 cells. *EMBO J.* 1993;12(2):749-758.

8. Vischer UM, Wagner DD. von Willebrand factor proteolytic processing and multimerization precede the formation of Weibel-Palade bodies. *Blood.* 1994;83(12):3536-3544.

9. Wise RJ, Barr PJ, Wong PA, Kiefer MC, Brake AJ, Kaufman RJ. Expression of a human proprotein processing enzyme: correct cleavage of the von Willebrand factor precursor at a paired basic amino acid site. *Proc Natl Acad Sci USA.* 1990; 87(23):9378-9382.

10. Wang JW, Valentijn KM, de Boer HC, et al. Intracellular storage and regulated secretion of von Willebrand factor in quantitative von Willebrand disease. *J Biol Chem.* 2011;286(27): 24180-24188.

11. Wang JW, Bouwens EA, Pintao MC, et al. Analysis of the storage and secretion of von Willebrand factor in blood outgrowth endothelial cells derived from patients with von Willebrand disease. *Blood.* 2013;121(14):2762-2772.

12. Starke RD, Paschalaki KE, Dyer CE, et al. Cellular and molecular basis of von Willebrand disease: studies on blood outgrowth endothelial cells. *Blood.* 2013;121(14):2773-2784.

13. Zenner HL, Collinson LM, Michaux G, Cutler DF. High-pressure freezing provides insights into Weibel-Palade body biogenesis. *J Cell Sci.* 2007; 120(Pt 12):2117-2125.

14. Lui-Roberts WW, Collinson LM, Hewlett LJ, Michaux G, Cutler DF. An AP-1/clathrin coat plays a novel and essential role in forming the Weibel-Palade bodies of endothelial cells. *J Cell Biol.* 2005;170(4):627-636.

15. Lui-Roberts WW, Ferraro F, Nightingale TD, Cutler DF. Aftiphilin and gamma-synergin are required for secretagogue sensitivity of Weibel-Palade bodies in endothelial cells. *Mol Biol Cell.* 2008;19(12):5072-5081.

16. Valentijn KM, Valentijn JA, Jansen KA, Koster AJ. A new look at Weibel-Palade body structure in endothelial cells using electron tomography. *J Struct Biol.* 2008;161(3):447-458.

17. Ferraro F, Kriston-Vizi J, Metcalf DJ, et al. A two-tier Golgi-based control of organelle size underpins the functional plasticity of endothelial cells. *Dev Cell.* 2014;29(3):292-304.

18. Hannah MJ, Skehel P, Erent M, Knipe L, Ogden D, Carter T. Differential kinetics of cell surface loss of von Willebrand factor and its propolypeptide after secretion from Weibel-Palade bodies in living human endothelial cells. *J Biol Chem.* 2005;280(24):22827-22830.

19. Valentijn KM, van Driel LF, Mourik MJ, et al. Multigranular exocytosis of Weibel-Palade bodies in vascular endothelial cells. *Blood.* 2010;116(10): 1807-1816.

20. Kukulski W, Schorb M, Welsch S, Picco A, Kaksonen M, Briggs JA. Correlated fluorescence and 3D electron microscopy with high sensitivity and spatial precision. *J Cell Biol.* 2011;192(1): 111-119.

21. Faas FGA, Avramut MC, van den Berg BM, Mommaas AM, Koster AJ, Ravelli RB. Virtual nanoscopy: generation of ultra-large high resolution electron microscopy maps. *J Cell Biol.* 2012;198(3):457-469.

22. Kobayashi K, Cheng D, Huynh M, Ratinac KR, Thordarson P, Braet F. Imaging fluorescently labeled complexes by means of multidimensional correlative light and transmission electron microscopy: practical considerations. *Methods Cell Biol.* 2012;111:1-20.

23. Bouwens EA, Mourik MJ, van den Biggelaar M, et al. Factor VIII alters tubular organization and functional properties of von Willebrand factor stored in Weibel-Palade bodies. *Blood.* 2011; 118(22):5947-5956.

24. Mastronarde DN. Automated electron microscope tomography using robust prediction of specimen movements. *J Struct Biol.* 2005;152(1):36-51.

25. Kremer JR, Mastronarde DN, McIntosh JR. Computer visualization of three-dimensional image data using IMOD. *J Struct Biol.* 1996; 116(1):71-76.

26. Holcomb PS, Hoffpauir BK, Hoyson MC, et al. Synaptic inputs compete during rapid formation of the calyx of Held: a new model system for neural development. *J Neurosci.* 2013;33(32): 12954-12969.